APPLICATION NOTE

AMETEK

Studying Solar Cells with the ModuLab XM PhotoEchem Optical and Electrical Measurment System

Application Note SA 105

Laurie Peter

Department of Chemistry

University of Bath

Bath BA2 7AY

United Kingdom

1st June 2016

1.Overview

The **ModuLab XM PhotoEchem** System was developed originally for the study of dye-sensitized solar cells, but because the system is so versatile it can be applied to other types of solar cells, notably to the new generation of hybrid organic-inorganic lead halide-based perovskite photovoltaics, which have achieved remarkable solar power conversion efficiencies of around 20%. The highly flexible Modulab system allows experimenters to perform a range of different measurements on solar cells or photoelectrochemical cells.

This technical note looks at the following methods:

- Impedance spectroscopy (in the dark and under illumination) (IS)
- Intensity-modulated photocurrent/photovoltage spectroscopy (IMPS/IMVS)
- Open circuit voltage decay measurements (OCVD)
- Charge extraction measurements (CE)

The objective of the note is to explain briefly the background to these techniques and to illustrate them with experimental results obtained with dye-sensitized solar cells and, more recently, with hybrid perovskite solar cells. The author is very grateful to Henry Snaith and Giles Eperon (Clarendon laboratory, Oxford), Petra Cameron (University of Bath) and Adam Pockett (Swansea University) for permission to use the perovskite results, which were obtained in a joint study that is being prepared for publication.

2. Impedance Spectroscopy of Solar Cells

2.1 Introduction

Impedance spectroscopy is a small amplitude measurement technique that involves application of a sinusoidal voltage or current to the system under study. Generally, the response of real systems including solar cells is *non-linear*, so the amplitude of the perturbing signal must be kept sufficiently small that the output signal can be described using the linear terms in a series expansion of the system response. In this case, the system can be represented using *linear R,C circuit elements*. In the case of solar cells, the impedance can be measured either in the dark or under illumination. In this technical note we look at two types of unconventional photovoltaic cells: dye-sensitized cells, and hybrid lead halide perovskite cells. For information on impedance studies of conventional silicon p-n cells or thin film solar cells such as CdS|CdTe, the interested reader is referred to papers by Mora-Sero et al.[1] and Friesen et al.[2] respectively.

2.2 Impedance response of dye-sensitized solar cells

The dynamic response of any solar cell depends on several key processes.

- charge transport
- charge storage
- electron-hole recombination
- interfacial charge transfer.

Constant illumination
0 V vs. open circuit
Small ac voltage modulation
1mHz – 1 MHz

Each of these processes can be reflected in the impedance response. We begin with the example of the dye-sensitized solar cell (DSSC) under illumination at open circuit, since in this particular case these processes can be separated quite easily using impedance

spectroscopy. The DSSC consists of a mesoporous TiO_2 layer covered by a monomolecular layer of light-harvesting dye. The mesoporous layer, which is deposited on a conducting glass substrate, is permeated by a redox electrolyte (e.g. I_3^-/I^-) or by a solid hole conductor (e.g. spiro-OMeTAD), and the thin cell is completed by a second contact: platinized conducting glass in the case of the original Grätzel cell[3] or an evaporated metal in the case of the solid state analogues using spiro-OMeTAD as a hole transport medium (HTM).[4] Typically, the mesoporous layer is around 1-15 microns thick, and the electrolyte gap is around 30-40 microns.

2.2.1 Processes in the DSSC

The processes taking place in a DSSC under working conditions are illustrated schematically in **Figure 1**. Excitation of dye molecules adsorbed on the mesoporous TiO_2 leads to injection of electrons into the oxide. The oxidized dye molecules then receive electrons from the iodide ions in solution, regenerating the dye and forming tri-iodide. The injected electrons hop through the network of interconnected TiO_2 particles to reach the conducting glass substrate and from there the external circuit. Meanwhile, the tri-iodide ions diffuse across the narrow gap to the platinized cathode, where they are accept electrons to form iodide, thereby completing the regenerative cycle.

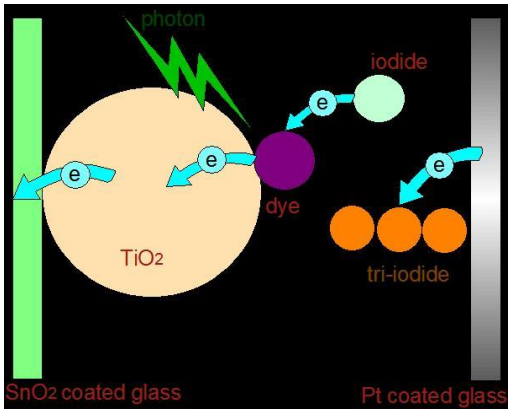

Figure 1. Simplified scheme illustrating the processes taking place in a DSSC under illumination at short circuit: electron injection from the photo-excited dye, regeneration of the dye by electron transfer from iodide ions, transport of electrons through the TiO_2 network, transport of I_3^- ions to the cathode and regeneration of iodide ions from I_3^- by electron transfer from the Pt cathode. Note that the back reaction of injected electrons with tri-iodide is not shown. At open circuit, the rate of this 'recombination' process exactly balances the rate of electron injection, determining the open circuit voltage. Only one TiO_2 particle is shown for simplicity (the mesoporous layer consists of many interconnected nanometer-sized particles).

2.2.2 Influence of trapping on the dynamic response of DSSCs

Illumination of the DSSC results in electron injection into the conduction band of the mesoporous TiO_2 layer, and the oxidized dye is rapidly recycled to its original reduced state by fast electron transfer from the electrolyte or spiro-OMeTAD phase. At open circuit, no current is extracted from the cell, so the electron injection process is balanced by the transfer of electrons back to the oxidized species in the contacting phase (i.e. to I_3^- in the electrolyte or to the radical cation (hole) in spiro-OMeTAD). The dynamic behavior of DSSCs is complicated by the fact that electrons can be captured by trap states located in the forbidden gap of the TiO_2. The exchange of electrons between trap states and the conduction band has a strong influence on the time constants associated with i) the transfer of electrons to the redox electrolyte (or hole transport phase) and ii) the transport of electrons through the DSSC. For a discussion of these effects see, e.g., refs [5-9].

The relaxation time associated with the loss of electrons to the redox electrolyte or HTM in a DSSC is generally referred to as the ***electron lifetime*** τ_n. This relaxation time depends on the occupancy of the exponential electron trap distribution in the mesoporous

TiO_2. The electron occupancy is determined by the **quasi Fermi level** (QFL) for electrons, ${}_nE_F$, which, under open circuit conditions, moves towards the conduction band with increasing illumination intensity as the concentration of electrons in the conduction band rises. The lifetime τ_n decreases as the QFL rises, and eventually when the QFL reaches the conduction band, τ_n should be equal to the lifetime of free electrons in the conduction band. In practice it is difficult, if not impossible, to reach this limit experimentally.

The relaxation time associated with electron transport in the DSSC is also affected by trapping/detrapping. This can be seen in the slow rise and fall of photocurrent transients. Electron transport in the DDSC occurs by diffusion, and the apparent **electron diffusion coefficient**, D_n, measured by transient or periodic methods depends on trap occupancy, i.e. on the QFL. D_n increases as the QFL rises towards the conduction band with increasing light intensity.

An important quantity for DSSC performance is the ***electron diffusion length***, given by $L_n = (D_n \tau_n)^{1/2}$, which is related to the average distance that electrons diffuse in the mesoporous titania layer before they are lost by transfer to the redox electrolyte or HTM. Conveniently, it turns out that L_n is independent of the QFL position since the QFL dependences of τ_n and D_n cancel out. The electron diffusion length, L_n, is one of the important parameters that can be obtained from the analysis of DSSC impedance.

2.2.3 Small signal equivalent circuit of the illuminated DSSC at open circuit

The equivalent circuit most widely used to model the impedance response of DSSCs was developed primarily by Juan Bisquert and his group (see http://www.elp.uji.es/). Its most important component is a **distributed impedance** or **finite transmission line** that represents electron transport and back reaction in the mesoporous oxide layer as well as the ability of the layer to store electron charge (primarily in the electron traps mentioned above). The ability of the semiconductor to store electronic charge defines the **chemical capacitance,** C_μ**,** of the cell. Additional elements in the case of the conventional electrolyte cell include the series resistance associated with the conducting glass substrate, the **Finite Warburg impedance** due to the diffusion of ions across the thin electrolyte gap, and finally the **Faradaic resistance** and **double layer capacitance** of the cathode. In the case where the cell is at open circuit under illumination, the gradients of electronic and ionic concentrations become negligible, so that the impedance behavior is simplified, since it is not necessary to take into account any distance dependence of the electron lifetime or charge storage. In practice this means that the distributed impedance can be represented by a series of identical RC elements as shown in **Figure 2**.

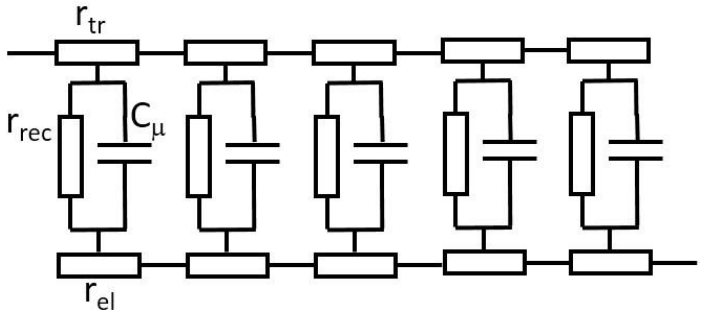

Figure 2. Distributed element or 'transmission line' representing the mesoporous TiO_2 layer in the DSSC. r_{tr} is the electron transport resistance, r_{rec} is the recombination resistance associated with back transfer of electrons to the redox system, r_{el} is the electrolyte resistance in the pores, C_μ is the chemical capacitance due to electron storage within the film (predominantly in electron traps). In many cases, r_{el} can be neglected. This distributed element is available in the ZView modelling

package (Scribner Associates) as Bisquert#3.

The relative values of r_{tr} and r_{rec} determine the electron diffusion length, L_n. The values of the total R_{tr} and R_{rec} obtained by fitting the impedance give the ratio of the electron diffusion length to the thickness of the mesoporous layer, d.

$$\frac{L_n}{d} = \sqrt{\frac{R_{rec}}{R_{tr}}} \qquad (1)$$

Impedance spectroscopy is therefore a useful method of determining L_n. Both R_{rec} and R_{tr} decrease with increasing intensity as a consequence of the exchange of electrons between traps and the conduction band in the mesoporous TiO_2 (the exact form of this intensity dependence is determined by the energetic distribution of traps). In order to guarantee good performance, R_{rec} needs to be considerably greater than R_{tr} so that all of the photo-injected electrons are collected, i.e. $L_n >> d$.

To obtain the equivalent circuit for the complete illuminated DSSC at open circuit, we need to add the series resistance, a finite Warburg element representing the transport of iodide and tri-iodide ions through the electrolyte as well as the Faradaic resistance and double layer capacitance of the cathode. If we represent the distributed circuit element as DX, the equivalent circuit shown in **Figure 3** can be used to model the impedance response.

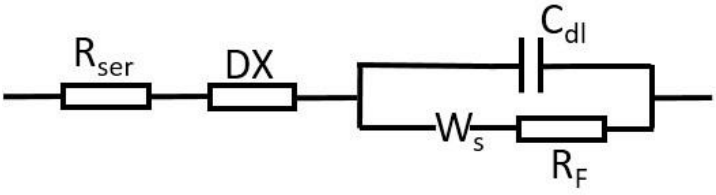

Figure 3. Complete equivalent circuit representing the impedance of an illuminated DSSC filled with a liquid redox electrolyte such as I^-/I_3^-. Here R_{ser} is the series resistance, W_s is the finite Warburg impedance associated with ion diffusion in the narrow gap, R_f is the Faradaic resistance for the I_3^-/I^- electrode process and C_{dl} is the double layer capacitance of the cathode. The transmission line impedance shown in Figure 2 has been simplified as DX.

The Warburg impedance for cells with low viscosity solvents such as acetonitrile is so small that it usually not possible to identify it in the impedance response. On the other hand, DSSCs fabricated with viscous ionic liquid electrolytes normally show a clear Warburg impedance when illuminated at intensities approaching 1 sun, where both R_{tr} and R_{rec} become small. A calculated example is shown in **Figure 4** to illustrate how the different components of the equivalent circuit are reflected in the impedance response. The values have been chosen to correspond to those for a typical cell containing an ionic liquid redox electrolyte in order that the Warburg impedance is visible.

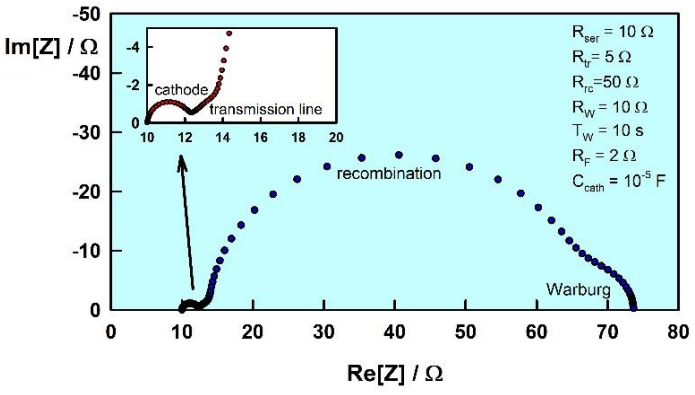

Figure 4. Impedance calculated for the equivalent circuit shown in Figure 3. The inset is an expansion of the high frequency response, which shows a semicircle due to the parallel combination of the cathode capacitance and faradaic resistance. This is followed by a short linear region with a slope of 45° that is due to the transmission line (DX) element. The large semicircle

arises from the parallel combination of R_{rec} and C_{μ}. The finite Warburg impedance can be seen in the low frequency response.

The three time constants associated with the cathode, recombination and ion diffusion can be seen in the phase angle plot in the Bode representation shown in **Figure 5**.

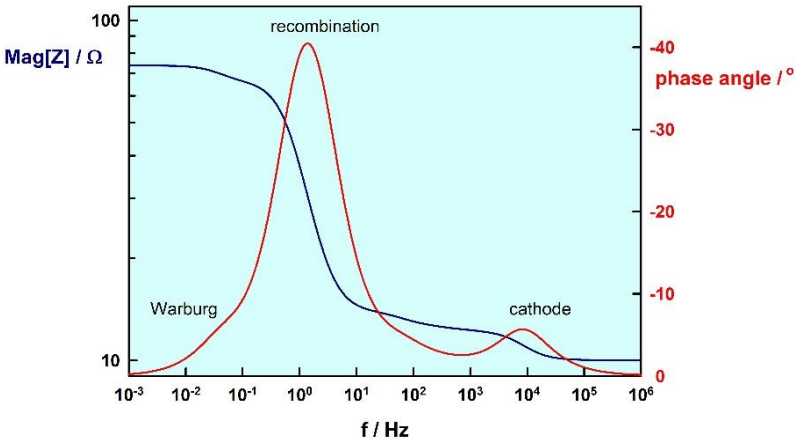

Figure 5. Bode plot corresponding to Figure 4. Note the very different time constants associated with electron transfer at the cathode, recombination (back transfer of electrons to the redox electrolyte), and the diffusion of ions across the small gap.

Further details of the impedance of DSSCs can be found in the extensive literature as well as in in chapters in reference [8].

2.3 Impedance Response of Planar Hybrid Perovskite Cells

The impedance response of hybrid lead halide perovskite solar cells is currently a hot topic, and there is as yet no agreed interpretation of the results. The measurement conditions discussed here are the same as those used for DSSCs, i.e. steady illumination and small amplitude modulation of the potential about the open circuit voltage. The results shown here are for cells that were fabricated by Giles Eperon in Henry Snaith's group at the Clarendon laboratory in Oxford and characterized by Adam Pockett in Bath. They consist of a thin (500-600 nm) layer of perovskite spin-coated onto FTO glass covered with a thin blocking layer of TiO_2. The perovskite is then coated with a layer of spiro-MeOTAD to act as hole acceptor, and the cell is finished with an evaporated metal layer. Measurements were carried out in a temperature-controlled dry atmosphere to prevent degradation affecting the results. The impedance response shown in **Figure 6** has a high frequency semicircle that is assigned to the parallel combination of the recombination resistance and the geometric capacitance of the thin perovskite film. The low frequency response seen in the impedance of perovskite solar cells has been interpreted in a number of different ways. Initially it was thought to correspond to a so-called giant dielectric effect in the perovskite,[10] but more recently this interpretation has lost favor. Other groups have assigned it to ionic migration or diffusion and have attempted to model it with a finite Warburg component by analogy with DSSCs.[11] Closer inspection of the plots suggests that a third time constant may be 'buried' in the transition between the high and low frequency arcs. This third time constant is resolved more clearly in the IMVS response, which is discussed in section 3.5.

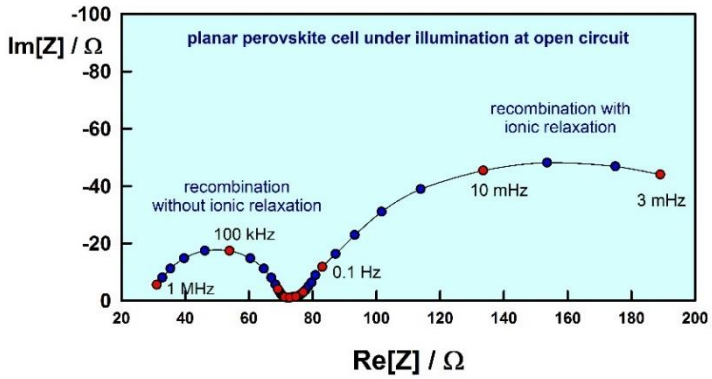

Figure 6. Typical impedance response of a planar hybrid perovskite solar cell under illumination at open circuit. The high frequency semicircle arises from the parallel combination of the geometric capacitance of the perovskite layer and the recombination resistance. The interpretation of the low frequency semicircle, which is controversial, is discussed below.

The remarkable separation between the time constants for the different processes is seen clearly in the Bode plot of the same impedance data (**Figure 7**). The results demonstrate the need to cover a very wide frequency range (9 decades) to capture all of the complex processes taking place.

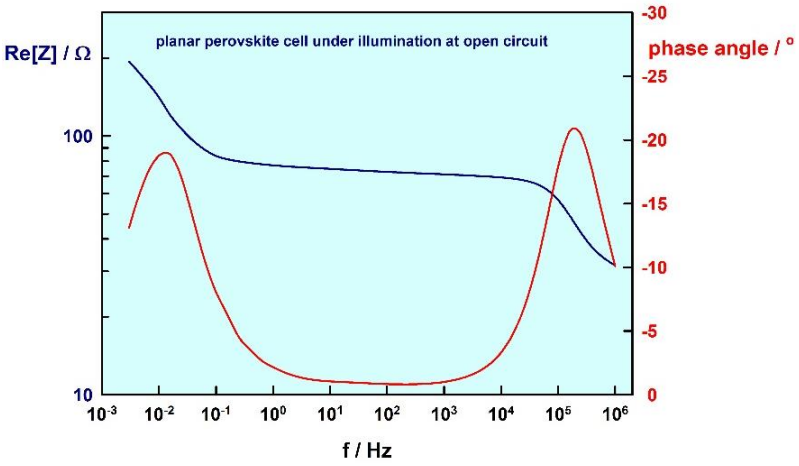

Figure 7. Bode plot corresponding to Figure 5. Note the very wide separation in the time constants of the two processes as reflected in the peaks in the phase angle.

Interestingly both semicircles in the impedance scale inversely with the illumination intensity as illustrated in **Figure 8**, indicating that they are both be coupled to electron-hole recombination.

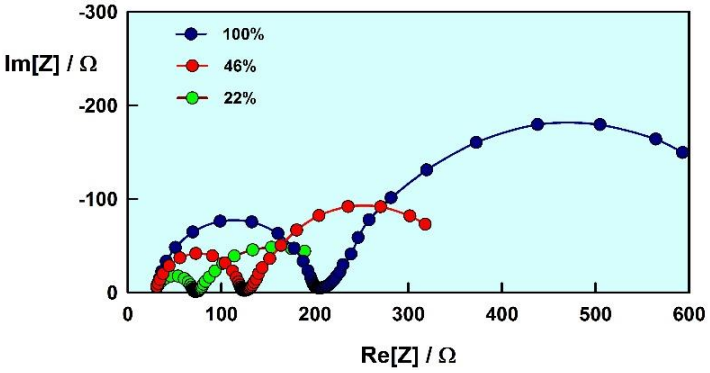

Figure 8. Impedance response of planar perovskite cell measured at three different relative illumination intensities. Note that the diameter of both semicircles decreases with intensity, showing that they are related to electron-hole recombination.

Our explanation of the impedance response of these planar perovskite solar cells is informed by the additional measurements carried out using the Modulab system, in particular intensity modulated photovoltage spectroscopy and open circuit voltage decay.

These are discussed below. It appears that one or more mobile ionic species are present in the perovskite layers. The most likely candidate is iodide vacancies, but methylammonium vacancies may also move. As a consequence, ionic double layers can form at the contacts. Perturbations of the voltage leads to movement of ions and corresponding changes in the potential distribution across the layer that affect the recombination rate. The time scale of this ionic relaxation is slow since it is related to the diffusion coefficients of the ionic defects concerned. It is important to note that the impedance seen at low frequencies is *not the ionic impedance itself*. Instead it represents the effect that ionic movement has on recombination. In effect, the recombination resistance becomes a complex impedance at low frequencies since the ions can respond to the electric field, and their movement modulates the recombination rate. In the example shown, the slowest relaxation time constant is of the order of 30s. This time constant can be related to ionic movement by the relationship $L_{diff} = (Dt)^{1/2}$, where D is the diffusion coefficient of the ionic defect and L_{diff} is the distance the ions move. Estimates of the diffusion coefficient of iodide vacancies at room temperature are around 10^{-12} cm^2 s^{-1}, so the corresponding diffusion or migration length would be around 50nm.

3. Intensity Modulated Photovoltage and Photocurrent Methods

3.1 Applications

IMVS (intensity modulated photovoltage spectroscopy) and IMPS (intensity modulated photocurrent spectroscopy) are closely related techniques in which the intensity of a light source (usually a light-emitting diode) is modulated by a few % and the response (current or voltage) is measured as a function of modulation frequency. IMPS and IMVS have been widely used to characterize electron transport and back reaction in mesoscopic dye-sensitized solar cells.[12-15] IMPS was originally developed to study photoelectrochemical reactions at the semiconductor/electrolyte interface,[16] and more recently it has been used to investigate the kinetics of light-driven water splitting reactions at semiconductor photoelectrodes.[17] However, both techniques have the potential to be applied to other types of solar cell, and both complement conventional impedance spectroscopy.

- IMVS normally at open circuit
- IMVS mainly gives information about recombination
- IMPS normally at short circuit
- IMPS gives mainly information about carrier transport

Steady illumination *plus*
Small amplitude modulated illumination
Open circuit for IMVS
Short circuit for IMPS

3.2 Basic Principles of IMVS and IMPS

The relationships between the modulated input photon flux function $\tilde{I}$ and the modulated current or voltage outputs are defined by the frequency-dependent **transfer functions**:

$$G_{IMVS}(\omega) = \frac{\tilde{U}_{photo}(\omega)}{\eta q \tilde{I}} \qquad G_{IMPS}(\omega) = \frac{\tilde{j}_{photo}(\omega)}{\eta q \tilde{I}} \tag{2}$$

Here the ~ symbol indicates the ac components of the variables. It can be seen that the IMPS transfer function is dimensionless, whereas the IMVS transfer function has units of Ω cm^2. This means that IMVS can be related to the impedance. The difference is that the controlled variable in impedance measurements is usually the ac voltage, whereas for IMVS it is essentially the internal current (no current flows through the external circuit).

3.3 IMPS and IMVS transfer functions for a photodiode

The simplest small amplitude equivalent circuit is this case is shown in **Figure 9**. It comprises a diode shunted by a parallel combination of a capacitor and a resistor. For open circuit conditions (i.e. measurement with a very high input impedance device like a voltage follower), R is the recombination resistance and C is the capacitance of the p-n junction at open circuit. For short circuit conditions, where recombination can normally be neglected, R represents the series resistance due to the contact resistance plus any (generally small) measuring resistance and C is the depletion capacitance at zero bias voltage. It can be seen that the current output of the diode at high frequencies will be attenuated by the RC time constant.

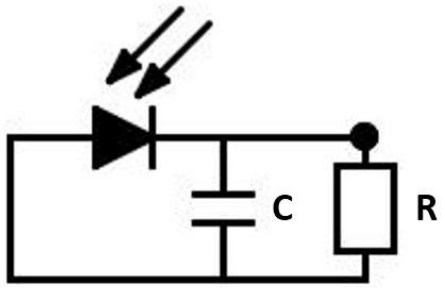

Figure 9. Simple small amplitude equivalent circuit of a photodiode or solar cell. For a p-n solar cell under open circuit conditions, C may be the chemical capitance of the device, and R is the recombination resistance. The product is related to the minority carrier lifetime(s) in the device. For fast p-i-n diodes, C is the much smaller geometric capacitance of the i-layer. Under short circuit conditions, C is determined by the junction capacitance and R is the total series resistance.

The IMVS response is an alternating voltage that arises from the internally generated photocurrent flowing through the parallel combination of capacitance and recombination resistance. If the quantum efficiency for photocurrent generation is η, then the IMVS response is given by

$$\tilde{U}_{photo}(\omega) = \eta q \tilde{I} R_{rec} \frac{1}{1 + j\omega RC} \tag{3}$$

where the second term represents the RC attenuation of the signal. For IMPS, the current measured in the external circuit has to pass through the measuring resistance, R, which is shunted by the capacitance, C, of the photodiode. This means that the measured ac current will be attenuated at high frequencies. The IMPS transfer function in this case is simply determined by the fraction of the current that flows through the resistive part of the circuit, and the IMPS transfer function is just

$$G_{IMPS}(\omega) = \frac{1}{1 + j\omega RC} \tag{4}$$

The frequency dependent parts of these two transfer functions can be broken down into real and imaginary parts and displayed in a complex plane plot. So, for example, the IMPS response is given by

$$\mathrm{Re}\left[G_{IMPS}(\omega)\right]=\frac{1}{1+\omega^2R^2C^2} \qquad \mathrm{Im}\left[G_{IMPS}(\omega)\right]=-\frac{j\omega RC}{1+\omega^2R^2C^2} \tag{5}$$

The response describes a semicircle in the lower complex plane as illustrated in **Figure 10**.

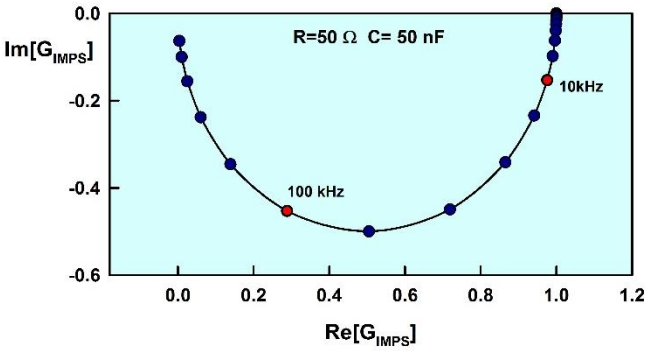

Figure 10. Complex plane plot of IMPS transfer function for a photodiode circuit (figure 9) with 50 Ω measuring resistor and a junction capacitance of 50 nF. The minimum of the semicircle appears at a radial frequency $\omega = 2\pi f = 1/RC = 4 \times 10^5\ s^{-1}$, which corresponds to f = 65 kHz.

The IMVS response is also semicircular, as illustrated in **Figure 11** (for simplicity) using the same values of R and C and a modulated photon flux of 10^{16} cm^{-2} s^{-1}. In this case, of course, R is the recombination resistance and not the measuring resistance.

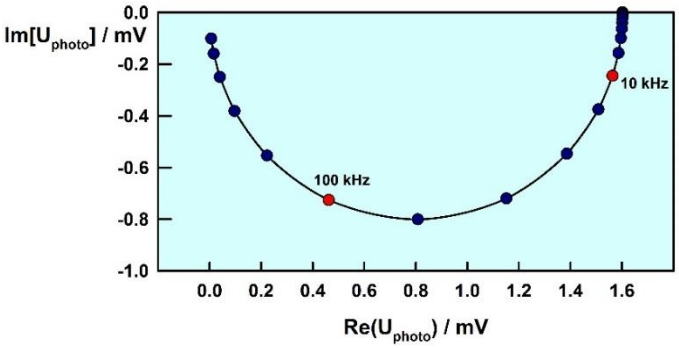

Figure 11. Complex plane plot of IMVS response calculated for the photodiode circuit (Figure 7) with R_{rec} = 50 Ω, C = 50 nF and a modulated photon flux of 10^{16} cm^{-2} s^{-1}. The quantum efficiency for photocurrent generation has been taken as η = 1.0. Note that the scaling factor for IMVS is $\eta q I R_{rec}$.

2.4 Use of IMPVS and IMPS to study Dye-Sensitized Solar Cells

IMVS has been widely used to measure the effective electron lifetime, τ_n in dye-sensitized solar cells. The method is straightforward, and the response is a semicircle with a minimum at the frequency given by the relationship $1/\tau_n = 2\pi f_{min}$. IMPS has been used to characterize electron transport in DSSCs. The response in this case is more complicated since it depends on the penetration depth of the incident light and on the direction of illumination (front or back). Exact analytical expressions are available for IMPS,[12] but they need to be convoluted with an RC attenuation function to take into account the phase shift introduced by the series resistance and electrode capacitance. Examples of calculated DSSC IMPS responses for illumination through the conducting glass substrate and for illumination through the cathode and electrolyte are shown in **Figure 12**.

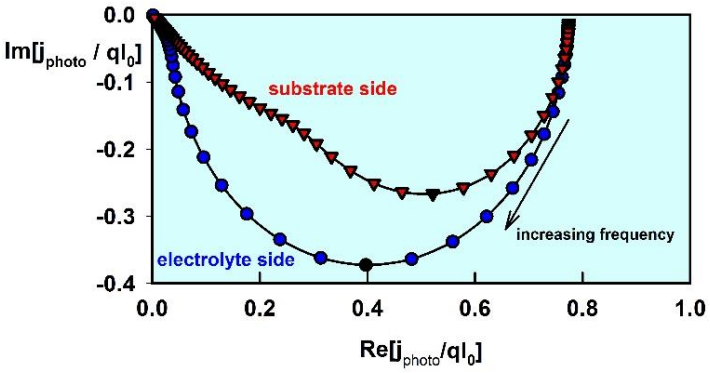

Figure 12. Examples of calculated IMPS responses for a DSSC for illumination through the conducting glass substrate and through the electrolyte side.

An experimental example of an IMPS response for illumination from the electrolyte side is shown in **Figure 13** for a dye-sensitized solar cell fabricated using 20 micron long TiO_2 nanotubes.[18] The data are fitted analytically to obtain the effective electron diffusion coefficient. Further details can be found in references [8, 19-20].

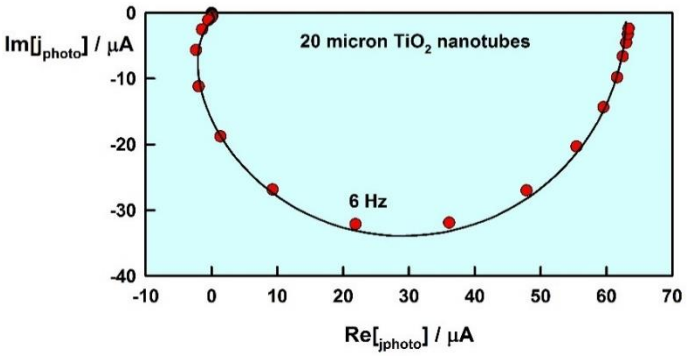

Figure 13. IMPS response for a dye-sensitized solar cell fabricated using 20 micron long dye-sensitized titania nanotubes. The line shows the fit to the data used to determine the effective electron diffusion coefficient in the titania nanotubes.

3.5 IMVS response of perovksite solar cells

IMVS has been used to study the complex processes involved in planar hybrid lead-halide perovskite solar cells.[21] The open circuit voltage of these cells is very high in relation to the bandgap of the material. This means that recombination losses are much lower than in most other semiconductors. It has become clear that theses perovskite materials are not only electronic conductors but also ionic conductors. It seems likely that the interaction between the ionic and electronic distributions may provide the mechanism for the voltage enhancement. Interestingly, the cell that shows two well-defined time constants in the impedance response (see section 1.3), gives *three* semicircles in the IMVS response. The IMVS transfer function as defined in section 2.2 can be obtained dividing the frequency-dependent ac photovoltage by the ac photocurrent measured at the open circuit voltage at low frequencies where the photocurrent is in phase with the illumination. **Figure 14** below illustrates the result, which shows the three clearly resolved semicircles.

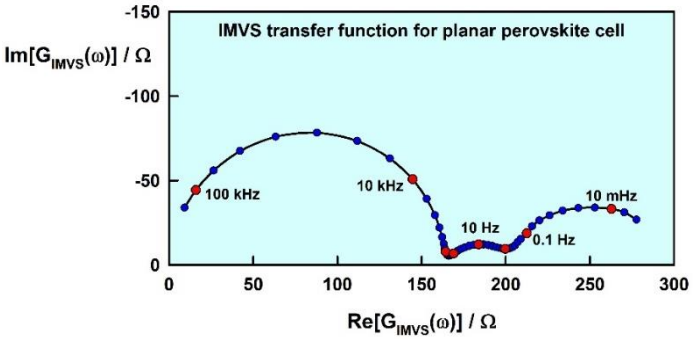

Figure 14. IMVS transfer function of a planar perovskite solar cell obtained by dividing the IMVS response by the ac photocurrent measured at low frequencies the open circuit potential

In principle, the IMVS transfer function should be identical with the impedance measured at open circuit under the same illumination conditions. Normally, IMVS responses are shown without scaling by the photocurrent, but this discards useful information. The comparison of the IMVS transfer function with the corresponding impedance response provides a useful test of the validity of the physical model. **Figure 15** shows such a comparison for a planar perovskite cell.

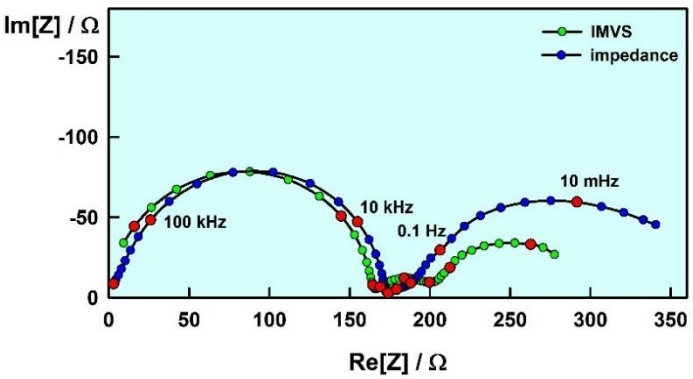

Figure 15. Compassion of IMVS transfer function (shown here simply as Z) with corresponding impedance response. In this particular case, the middle semicircle is clearly resolved in the IMVS, whereas it is less obvious in the impedance plot. Note the close correspondence between the two plots except at low frequencies, where the impedance arc is larger than the IMVS arc. This may be due to small changes in the cell performance with time.

4. Open Circuit Voltage Decay (OCVD)

The previous techniques all utilize small amplitude perturbations in order to linearize the system response in the frequency domain. Linearization is obviously convenient when one wants to model a system in terms of linear circuit elements (resistors and capacitors), but it is necessary to repeat measurements at a series of dc potentials or dc illumination intensities to fully characterize a non-linear system such as a solar cell. An alternative approach that can be realized using the Modulab system involves applying a large amplitude perturbation (voltage, current or illumination) and measuring the system response in the time domain. The most useful large-amplitude technique for the study of DSSCs and perovskite solar cells is the open circuit decay method, which convolves illuminating the solar cell at open circuit to establish a steady state open circuit voltage and then interrupting the illumination. The subsequent decay of open circuit voltage is the measured using an ultra-high impedance amplifier. The method was originally developed for conventional silicon solar cells, where under certain conditions the voltage decay gives information about the minority carrier lifetime, which is typically in the microsecond region. More recently is has been applied to DSSCs and hybrid perovskite solar cells.[22]

4.1 OCVD of DSSCs

In the case of DSSCs, the decay of open circuit voltage is remarkably slow: the cell may require several *minutes* to return to zero volts. The reason for this is that the voltage is controlled by the concentration of electrons in the mesoporous titania film. Most of these are located in trap states located in the forbidden gap of the oxide. The loss of these electrons by transfer to redox species (e.g. I_3^-) in the electrolyte is retarded by the slow thermal emission of electrons from traps to the conduction band (the deeper the traps, the slower the emission process). Electrons can also be transferred via the fluorine-doped tin oxide (FT)) coated glass substrate. This 'shunting' of the DSCC is not important for the original type of Grätzel cells containing iodide/tri-iodide redox couple, but if faster redox systems or hole conducting materials are used, it can become the major loss mechanism. **Figure 16** contrasts the decay curves for DSSCs with and without a thin blocking layer of titania underneath the porous layer. It can be seen that the decay in the absence of the blocking layer is complete in 10s, whereas the decay in the presence of the blocking layer is so slow that V_{oc} is still around 0.3 V after 20s (in fact, the complete decay takes several minutes)

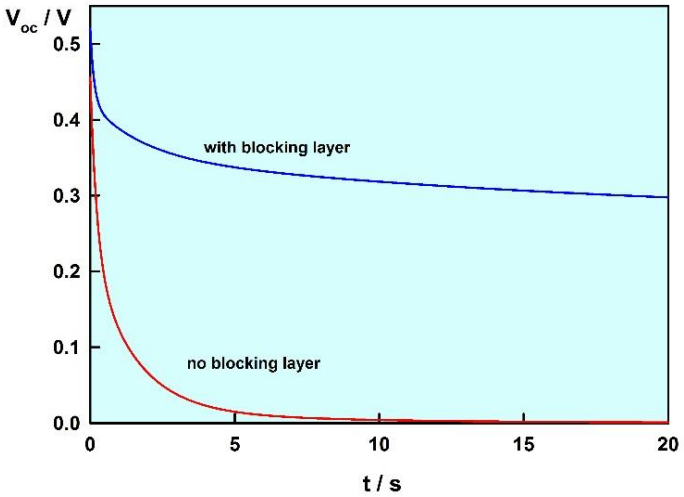

Figure 16. Open circuit voltage decays of DSSCs with and without a compact TiO_2 blocking layer to prevent back reaction of electrons with tri-iodide ions in the electrolyte occurring via the conducting glass substrate (shunting). In the presence of the blocking layer, electron transfer occurs only from the conduction band of the mesoporous layer (a much slower process). The plots show only the 'off' part of the transients obtained using a square illumination pulse.

The voltage decay provides information about the energetic distribution of electron traps in the forbidden gap of the mesoporous TiO_2. This distribution corresponds to an exponential decrease of the concentration of traps per unit energy going from the conduction band edge down into the forbidden gap. For further information about the theory of OCVD for DSSCs, the interested reader is directed to ref [22].

3.2 Charge extraction measurements with DSSCs

The extraordinarily high concentrations of trapped electrons in DSSCs (up to 10^{19} cm^{-3}) can be measured using a technique known as charge extraction. This involves illuminating the cell at open circuit to fill the traps below the quasi-Fermi level, which corresponds to the open circuit voltage. The illumination is then switched off and the voltage is allowed to decay for a pre-determined time, after which the cell is short circuited and electrons flow into the external circuit. The current 'spike' associated with release of trapped electrons is integrated over a suitable period (typically tens of seconds) to determine the trapped charge as shown in **Figure 17**.

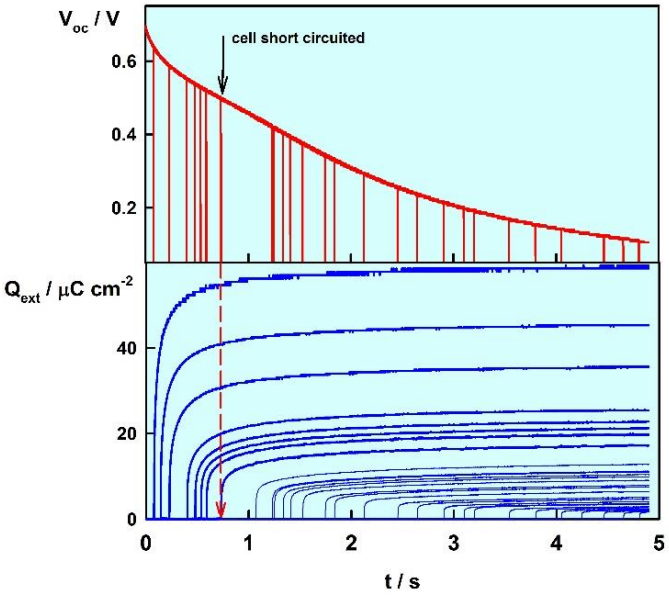

Figure 17. Charge extraction plots for a typical DSSC. The upper set of traces shows a series of open circuit voltage decays that are interrupted at different times by short circuiting the cell. The lower set of traces show the corresponding integrated current 'spikes' that give the extracted charge as a function of the open circuit voltage at the point at which the cell is short circuited. The arrow highlights one example, showing how the charge extraction plot builds up measured immediately after short circuiting the cell.

The experiment is then repeated with progressively longer decay times to obtain the trapped electron concertation as a function of open circuit voltage, and hence of the quasi Fermi level position. It is important to note that it is assumed that no electrons are lost by transfer to the electrolyte during the charge extraction process. This means that the electron diffusion length needs to be greater than the film thickness. If this criterion is not met, the extracted charge will be lower than the trapped charge. More details can be found in ref [23].

The extracted charge is then plotted as a function of the open circuit voltage at which the cell was short circuited as shown in **Figure 18**. The charge can then be converted into an electron concentration using the known thickness and porosity of the mesoporous titania layer.

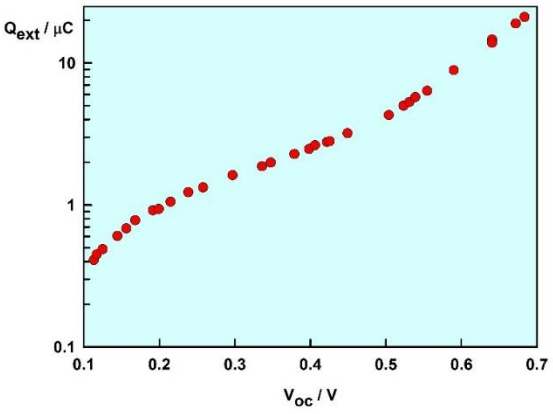

Figure 18. Extracted charge plotted as a function of the open circuit voltage at which the cell was short circuited to allow the electrons to escape to the external circuit**.** The plot is then used to drive the trap distribution as a function of energy.

3.3 OCVD of planar perovskite cells

Interestingly, the open circuit voltage decay of planar perovskite cells has a very slow component following an initial much more rapid decay, as shown in **Figure 19**.

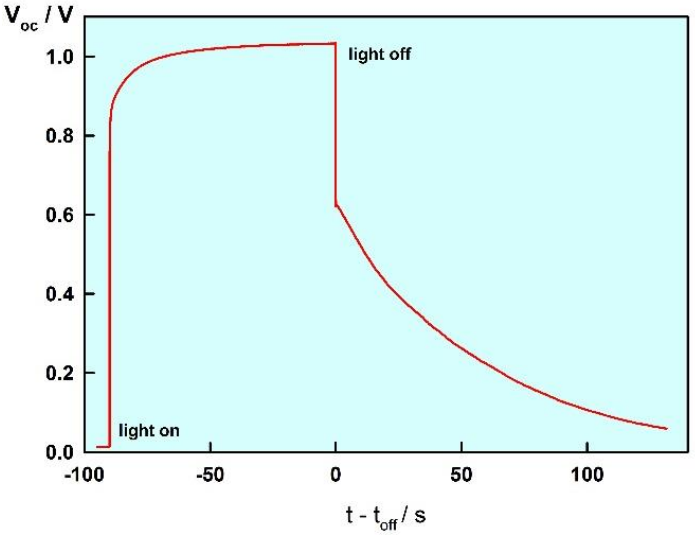

Figure 19. Open circuit voltage transient showing very high voltages achieved by a planar perovskite solar cell. The open circuit voltage decay is initially fast, but when the voltages reaches about 0.6 V, the decay slows substantially, and several minutes are required before V_{oc} reaches zero. Note also the slow rise to the maximum open circuit voltage after the illumination is switched on.

The difference in time scales between the initial and final decay can be appreciated better when a logarithmic time axis is used, as shown in **Figure 20**. The initial rapid decay occurs on a time scale of milliseconds, whereas the slow decay requires tens of seconds. Both of these time scales are much longer than expected for a simple p-i-n device in which the electron/hole lifetimes are more likely on a nanosecond to microsecond time scale. It appears that illumination results in a change in the internal electrical field in the thin (ca 500 nm) perovskite layer, resulting in the movement of ion vacancies (probably iodide vacancies). The movement of ions is associated with the formation of electrical double layers at the contacts. Further discussion is beyond the scope of this technical note, but it is clear that the OCVD techniques is a valuable method for the study of complex systems.

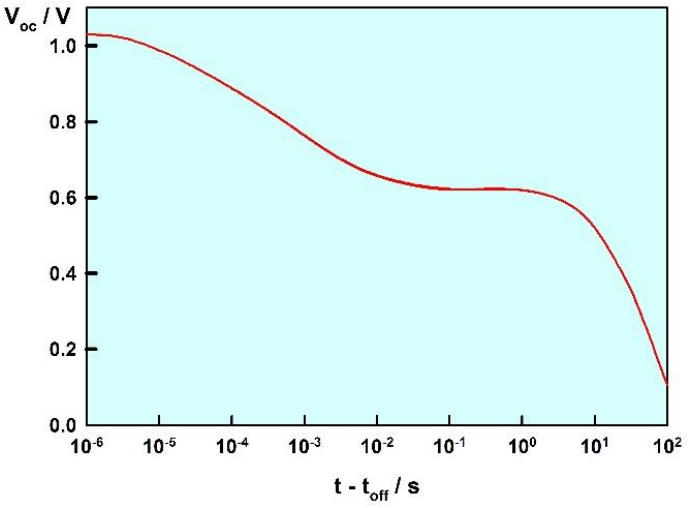

Figure 20. OCVD plotted on a logarithmic time scale illustrating two different time regions for the voltage decay. Clearly the decay is much more complicated than expected for a simple p-i-n photodiode structure. The evidence suggest that two relaxation regions are the same as those seen in the IMVS response seen in Figure 14. In both cases, the relaxation mechanism involves the movement of ion vacancies in the methylammonium lead iodide.

References

1. Mora-Sero, I.; Garcia-Belmonte, G. A.; Boix, P. P.; Vazquez, M. A.; Bisquert, J., Impedance Spectroscopy Characterisation of Highly Efficient Silicon Solar Cells under Different Light Illumination Intensities. *Energy & Environmental Science* **2009**, *2*, 678-686.
2. Friesen, G.; Dunlop, E. D.; Wendt, R., Investigation of Cdte Solar Cells Via Capacitance and Impedance Measurements. *Thin Solid Films* **2001**, *387*, 239-242.
3. O'Regan, B.; Grätzel, M., A Low-Cost, High-Efficiency Solar-Cell Based on Dye-Sensitized Colloidal Tio2 Films. *Nature* **1991**, *353*, 737-740.
4. Bach, U.; Lupo, D.; Comte, P.; Moser, J. E.; Weissortel, F.; Salbeck, J.; Spreitzer, H.; Grätzel, M., Solid-State Dye-Sensitized Mesoporous TiO_2 Solar Cells with High Photon-to-Electron Conversion Efficiencies. *Nature* **1998**, *395*, 583-585.
5. Peter, L.M., "Sticky Electrons" Transport and Interfacial Transfer of Electrons in the Dye-Sensitized Solar Cell. *Acc Chem Res* **2009**, *42*, 1839-47.
6. Peter, L. M., Characterization and Modeling of Dye-Sensitized Solar Cells. *Journal of Physical Chemistry C* **2007**, *111*, 6601-6612.
7. Peter, L. M., Dye-Sensitized Nanocrystalline Solar Cells. *PCCP* **2007**, *9*, 2630-2642.
8. Hagfeldt, A.; Peter, L. M., Characteriztion and Modeling of Dye-Sensitized Solar Cells: A Toolbox Approach. In *Dye Sensitized Solar Cells*, Kalyanasundaranam, K., Ed. EPFL Press: Lausanne, 2010; pp 457-554.
9. Bisquert, J.; Vikhrenko, V. S., Interpretation of the Time Constants Measured by Kinetic Techniques in Nanostructured Semiconductor Electrodes and Dye- Sensitized Solar Cells. *J. Phys. Chem. B* **2004**, *108*, 2313-2322.
10. Juarez-Perez, E. J.; Sanchez, R. S.; Badia, L.; Garcia-Belmonte, G.; Kang, Y. S.; Mora-Sero, I.; Bisquert, J., Photoinduced Giant Dielectric Constant in Lead Halide Perovskite Solar Cells. *The Journal of Physical Chemistry Letters* **2014**, *5*, 2390-2394.
11. Bag, M.; Renna, L. A.; Adhikari, R. Y.; Karak, S.; Liu, F.; Lahti, P. M.; Russell, T. P.; Tuominen, M. T.; Venkataraman, D., Kinetics of Ion Transport in Perovskite Active Layers and Its Implications for Active Layer Stability. *J. Am. Chem. Soc.* **2015**, *137*, 13130-13137.
12. Dloczik, L.; Ileperuma, O.; Lauermann, I.; Peter, L. M.; Ponomarev, E. A.; Redmond, G.; Shaw, N. J.; Uhlendorf, I., Dynamic Response of Dye-Sensitized Nanocrystalline Solar Cells: Characterization by Intensity-Modulated Photocurrent Spectroscopy. *J. Phys. Chem. B* **1997**, *101*, 10281-10289.
13. Fisher, A. C.; Peter, L. M.; Ponomarev, E. A.; Walker, A. B.; Wijayantha, K. G. U., Intensity Dependence of the Back Reaction and Transport of Electrons in Dye-Sensitized Nanacrystalline Tio2 Solar Cells. *J. Phys. Chem. B* **2000**, *104*, 949-958.
14. Ponomarev, E. A.; Peter, L. M., A Generalized Theory of Intensity-Modulated Photocurrent Spectroscopy (IMPS). *J. Electroanal. Chem.* **1995**, *396*, 219-226.
15. Ponomarev, E. A.; Peter, L. M., A Comparison of Intensity Modulated Photocurrent Spectroscopy and Photoelectrochemical Impedance Spectroscopy in a Study of Photoelectrochemical Hydrogen Evolution at P-InP. *J. Electroanal. Chem.* **1995**, *397*, 45-52.
16. Peat, R.; Peter, L. M., Characterization of Semiconductor Electrodes by Intensity Modulated Spectroscopy (IMPS). *J. Electrochem. Soc.* **1986**, *133*, C334.
17. Peter, L. M., Energetics and Kinetics of Light-Driven Oxygen Evolution at Semiconductor Electrodes: The Example of Hematite. *J. Solid State Electrochem.* **2013**, *17*, 315-326.
18. Jennings, J. R.; Ghicov, A.; Peter, L. M.; Schmuki, P.; Walker, A. B., Dye-Sensitized Solar Cells Based on Oriented Tio2 Nanotube Arrays: Transport, Trapping, and Transfer of Electrons. *J. Am. Chem. Soc.* **2008**, *130*, 13364-13372.
19. Peter, L. M.; Vanmaekelbergh, D., Time and Frequency Resolved Studies of Photoelectrochemical Kinetics. In *Adv. Electrochem. Sci. Eng.*, Alkire, R. C. and Kolb, D.M., Ed. Weinheim, 1999; Vol. 6, pp 77-163.

20. Peter, L. M., Tributsch, H., Experimental Techniques in Photoelectrochemistry. In *Nanostructured and Photoelectrochemical Systems for Solar Photon Conversion*, Archer, M. D. and Nozik, A.J, Ed. Imperial College Press: London, 2008; Vol. 3, pp 675-736.

21. Pockett, A. C., Cameron,P.J., Peter, L.M., Eperon, G.E., Snaith, H.J.. In Preparation. **2016**.

22. Walker, A. B.; Peter, L. M.; Lobato, K.; Cameron, P. J., Analysis of Photovoltage Decay Transients in Dye-Sensitized Solar Cells. *J. Phys. Chem. B* **2006**, *110*, 25504-25507.

23. Duffy, N. W.; Peter, L. M.; Rajapakse, R. M. G.; Wijayantha, K. G. U., A Novel Charge Extraction Method for the Study of Electron Transport and Interfacial Transfer in Dye Sensitised Nanocrystalline Solar Cells. *Electrochem. Commun.* **2000**, *2*, 658-662.